Towards Multiple Missing Values-resistant Unsupervised Graph Anomaly Detection

Jiazhen Chen^{1*}, Xiuqin Liang^{2*}, Sichao Fu^{3,4†}, Zheng Ma⁵, Weihua Ou⁶

¹Department of Statistics and Actuarial Science, University of Waterloo

²Data Science Center of Excellence, Deloitte Consulting Beijing

³School of Electronic Information and Communications, Huazhong University of Science and Technology

⁴ Text Computing and Cognitive Intelligence Ministry of Education Engineering Research Center, Guizhou University

⁵Cheriton School of Computer Science, University of Waterloo

⁶School of Big Data and Computer Science, Guizhou Normal University

j385chen@uwaterloo.ca, pliang@deloittecn.com.cn, fusichao_upc@163.com, z43ma@uwaterloo.ca, ouweihua@gznu.edu.cn

Abstract

Unsupervised graph anomaly detection (GAD) has received increasing attention in recent years, which aims to identify data anomalous patterns utilizing only unlabeled node information from graph-structured data. However, prevailing unsupervised GAD methods typically presuppose complete node attributes and structure information, a condition hardly satisfied in real-world scenarios owing to privacy, collection errors or dynamic node arrivals. Existing standard imputation schemes risk "repairing" rare anomalous nodes so that they appear normal, thereby introducing imputation bias into the detection process. In addition, when both node attributes and edges are missing simultaneously, estimation errors in one view can contaminate the other, causing cross-view interference that further undermines the detection performance. To overcome these challenges, we propose M²V-UGAD, a multiple missing values-resistant unsupervised GAD framework on incomplete graphs. Specifically, a dual-pathway encoder is first proposed to independently reconstruct missing node attributes and graph structure, thereby preventing errors in one view from propagating to the other. The two pathways are then fused and regularized in a joint latent space so that normals occupy a compact inner manifold while anomalies reside on an outer shell. Lastly, to mitigate imputation bias, we sample latent codes just outside the normal region and decode them into realistic node features and subgraphs, providing hard negative examples that sharpen the decision boundary. Experiments on seven public benchmarks demonstrate that M²V-UGAD consistently outperforms existing unsupervised GAD methods across varying missing rates.

1 Introduction

Graph-structured data is pervasive across various real-world domains, including social networks, financial transaction systems, e-commerce platforms, and biological interaction networks (Chaudhary, Mittal, and Arora 2019; Huang et al. 2022; Zhang et al. 2022; Chen et al. 2025; Yu et al. 2024,

Copyright © 2026, Association for the Advancement of Artificial Intelligence (www.aaai.org). All rights reserved.

2025). While these graph-structured data are adept at capturing rich and complex relationships among entities, they are frequently contaminated by anomalous patterns. For example, collusive users may inflate or deflate item ratings to manipulate ranking algorithms; whereas in social-media graphs, spam accounts frequently coalesce into unusually dense connectivity clusters (Fakhraei et al. 2015; Zhang et al. 2020). Graph anomaly detection (GAD) seeks to isolate these irregular nodes by identifying attribute profiles or structural patterns that diverge markedly from the dominant graph distribution. Nevertheless, the effectiveness of GAD is often hindered by extreme class imbalance and the scarcity of reliable labels: true anomalies are vastly outnumbered by normal nodes, and acquiring ground-truth annotations is both costly and often impractical (Ma et al. 2021). These challenges have propelled recent research toward unsupervised GAD, where detectors must discern abnormality solely from the unlabeled graph-structured data.

Unsupervised GAD seeks to effectively spot nodes or substructures that violate the graph's intrinsic attributes or topological regularities, operating on the premise that anomalies stand apart from normal patterns. Existing work falls largely into two families: reconstruction-based approaches and contrastive-learning approaches. Reconstruction-based methods train graph autoencoders to recover node attributes or structure and detect anomalies by measuring reconstruction errors (Ding et al. 2019a; Luo et al. 2022; He et al. 2024; Li et al. 2025). For instance, ADA-GAD (He et al. 2024) pretrains multi-level graph autoencoders on spectral anomalydenoised augmented graphs, then reconstructs the original graph and uses the resulting attribute and structure reconstruction errors to identify anomalies. DiffGAD (Li et al. 2025) leverages latent diffusion models to distill discriminative and common information in node representations, then reconstructs the original graph and uses reconstruction errors in the latent space to detect anomalies.

On the other hand, contrastive learning-based methods distinguish anomalies by learning to separate normal and abnormal patterns through agreement or disagreement between node representations and their local neighborhoods (Liu et al. 2022; Pan et al. 2023; Jin et al. 2021; Duan et al. 2023;

^{*}These authors contributed equally.

[†]Corresponding author.

Chen et al. 2024). For example, CoLA (Liu et al. 2022) formulates anomaly detection as a node-versus-subgraph contrastive task, training a GNN to distinguish normal from abnormal nodes according to the agreement between node representations and their local subgraphs. PREM (Pan et al. 2023) pre-aggregates ego-neighbor features with a single anonymized message-passing step, then uses a simple contrastive matching network to efficiently score anomalies according to ego-neighbor representation similarity.

Despite their efficacy, existing unsupervised GAD methods implicitly assume a complete input graph-structured data, i.e., one in which both the node feature matrix is complete and the adjacency matrix captures the full topology. Nevertheless, both the node attributes and edge connectivity are often missing in practice: node attributes may be redacted for privacy or lost in acquisition; node edges may be missing when new nodes arrive or when interactions go unrecorded (Xia et al. 2025). A typical remedy is to perform data imputation before anomaly detection. Off-the-shelf imputers like Mean, MissForest (Stekhoven and Bühlmann 2011) or GAIN (Yoon, Jordon, and van der Schaar 2018) treat each node in isolation, thus ignoring the relational cues that become critical under severe missingness. More recent graph-aware imputers exploit the observed topology to guide node attribute reconstruction: some match the distributions of node attribute and structure embeddings (Jiang et al. 2024; Chen et al. 2020), others refine structure-derived embeddings iteratively to impute missing features (Tu et al. 2022), or restrict message passing to observed attributes only (Jiang and Zhang 2020). Yet these techniques hinge on reciprocal complementation between the node attribute and structural views; when either view is incomplete, noise in one bleeds into the other. Recent studies reveal that this cross-view interference amplifies reconstruction errors and ultimately degrades the resulting node representations (Huo et al. 2023; Fu et al. 2023). Some approaches mitigate this by decoupling attribute imputation from structure enhancement before alignment (Huo et al. 2023; Yuan and Tang 2024). However, they heavily rely on partial label supervision for node classification and are therefore unsuitable for a fully unsupervised anomaly detection task.

Aside from the mutual interference arising from dual feature-structure incompleteness, another critical challenge is the imputation bias issue, which arises due to the rarity of anomalies. In a conventional two-stage (impute-then-detect) pipeline, the imputer is trained almost exclusively on nodes that exhibit normal behaviour. As a result, it fills missing attributes or absent edges with prototypical normal values during inference. This process suppresses the distinctive patterns that characterise anomalies and pulls them toward the distribution of normal nodes, and consequently masks them from the detector. Recent empirical studies demonstrate that the more faithfully an imputer reproduces normal patterns, particularly when the proportion of missing data is low, the more pronounced this bias becomes. Ultimately, it leads to degradation in anomaly-detection performance (Xiao and Fan 2024; Zemicheal and Dietterich 2019).

In this work, we propose an unsupervised anomaly detection framework robust to graphs with incomplete node

attributes and topology, termed M²V-UGAD. The framework is specifically designed to tackle cross-view interference and imputation bias under anomaly scarcity arising in the incomplete-graph setting. To correctly impute data while preventing errors from propagating between the attribute and structural views, we introduce a dual-pathway encoder that independently imputes node features via an MLP and restores missing edges through deterministic Personalized PageRank diffusion. To allow the reconstructed two views to complement one another, we fuse them in a shared latent space using a lightweight GCN. A Sinkhorn divergence further regularizes the embeddings toward a truncated hyperspherical Gaussian, ensuring a compact normal region and clear separation of anomalies. To preserve intricate attribute-structure semantics and avoid collapse of the normal region, we append a recovery decoder that reconstructs node features from the latent embeddings, enforcing semantic consistency. To counteract imputation bias under anomaly scarcity, we synthesize pseudo-anomalies by sampling latent codes just beyond the normal region, and decoding them into realistic features and an internally connected subgraph. Thus providing challenging and plausible contrastive examples. Finally, to reinforce a clear boundary between normal nodes and anomalies, we fine-tune with a mixed Sinkhorn loss, ensuring normals remain tightly clustered while pseudo-anomalies are aligned to the outer ring.

The main contributions are summarized as follows:

- **Novel Problem:** To the best of our knowledge, we are the first to investigate and address the problem of unsupervised GAD in the setting where both node attributes and the underlying topology are incomplete.
- Dual-pathway Imputation and Hyperspherical Fusion: To avoid error propagation while exploiting complementary signals, we disentangle attribute and topology imputation via a dual-pathway module and fuse the two restored views under a truncated hyperspherical Gaussian prior. A reconstruction constraint is enforced to preserve fine-grained attribute–structure semantics.
- **Graph Pseudo-anomaly Generation:** To counteract imputation bias and fortify the anomaly frontier, we sample latent codes from the ring-shaped shell beyond the normal manifold, decode them into realistic pseudo-anomaly nodes and a self-contained subgraph, and enforce their separation via mixed Sinkhorn divergence.
- Extensive Empirical Validation: Experiments on seven public benchmarks show the superior performance of M²V-UGAD over existing unsupervised GAD methods across varying missing rates.

2 Methodology

2.1 Overview

This section gives an overview of the M²V-UGAD framework (see Figure 1), which tackles unsupervised GAD with incomplete attributes and topology. To handle missing features and edges without mutual interference, a dual-pathway imputation module independently reconstructs node attributes via an MLP encoder and restores missing edges

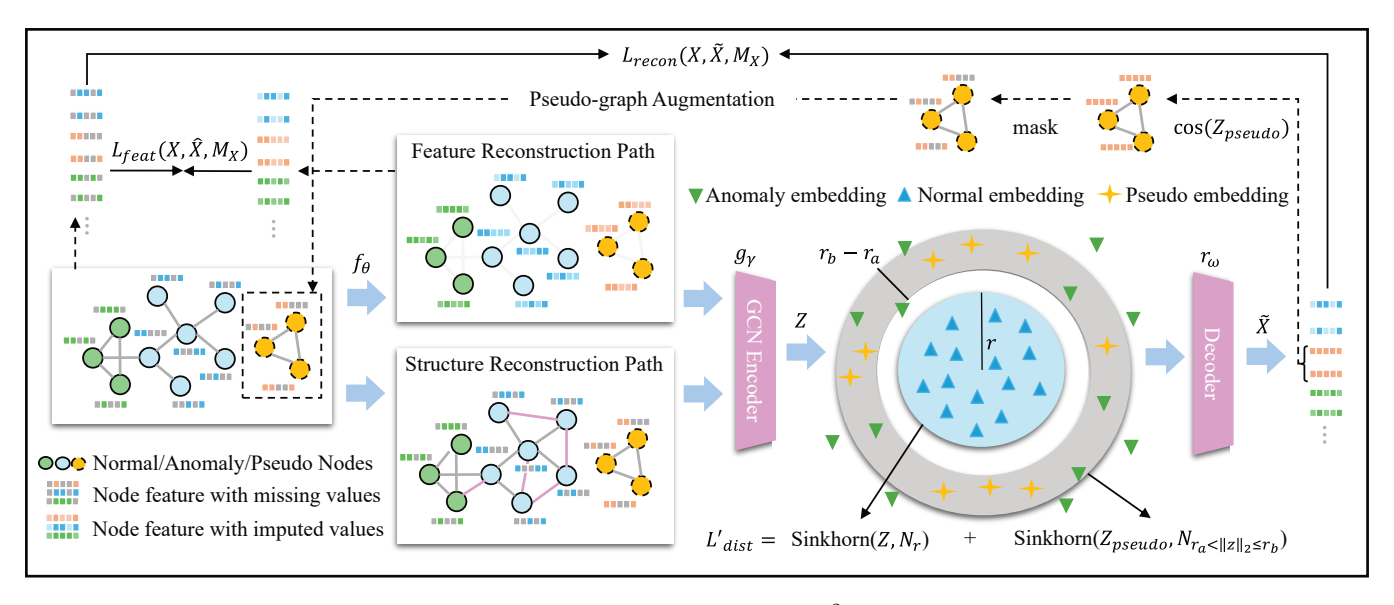


Figure 1: A diagram illustrating the proposed M²V-UGAD framework.

via deterministic Personalized PageRank diffusion (Section 2.3). These two reconstructions are projected into a shared latent space, where a Sinkhorn divergence aligns the empirical distribution to a truncated Gaussian on a hypersphere, and a recovery decoder reconstructs node attributes to preserve attribute–structure semantics (Section 2.4). Finally, to mitigate imputation bias from anomaly scarcity, the model is fine-tuned on an augmented dataset that includes pseudo-anomalies sampled from the ring-shaped shell beyond the normal latent sphere (Section 2.5). The full training pipeline and anomaly scoring are detailed in Section 2.6.

2.2 Problem Formulation

Consider an undirected attributed graph $\mathcal{G} = (\mathcal{V}, \mathcal{E}, \mathbf{X})$, where $\mathcal{V} = \{v_1, \dots, v_n\}$ denotes the set of nodes, $\mathcal{E} \subseteq \mathcal{V} \times \mathcal{V}$ denotes the set of edges, and $\mathbf{X} = [\mathbf{x}_1; \dots; \mathbf{x}_n] \in \mathbb{R}^{n \times d}$ is the node attribute matrix, with $\mathbf{x}_i \in \mathbb{R}^d$ representing the attributes of node v_i . The graph topology is encoded by a binary symmetric adjacency matrix $\mathbf{A} \in \{0,1\}^{n \times n}$, where $\mathbf{A}_{ij} = 1$ if and only if $(v_i, v_j) \in \mathcal{E}$.

Incomplete observations In practice, both node attributes and edges may be partially missing, yielding incomplete observations $\mathcal{G}_{\text{obs}} = (\mathcal{V}, \mathcal{E}_{\text{obs}}, \mathbf{X}_{\text{obs}})$, where $\mathcal{E}_{\text{obs}} \subseteq \mathcal{E}$ and \mathbf{X}_{obs} is the incomplete attributes and adjacency structure are described by $\mathbf{M}_X \in \{0,1\}^{n \times d}$ and $\mathbf{M}_A \in \{0,1\}^{n \times n}$, respectively, as $\mathbf{X}_{\text{obs}} = \mathbf{M}_X \odot \mathbf{X}$, $\mathbf{A}_{\text{obs}} = \mathbf{M}_A \odot \mathbf{A}$, where \odot denotes the element-wise product. Unobserved entries in \mathbf{X}_{obs} and \mathbf{A}_{obs} (i.e., entries with mask values of 0) are initially zero-filled and serve as placeholders during preprocessing.

Objective Under the majority-normal assumption, the objective is to learn an anomaly-scoring function $f: (\mathbf{X}_{\text{obs}}, \mathbf{A}_{\text{obs}}, \mathbf{M}_X, \mathbf{M}_A) \to \mathbf{s} \in \mathbb{R}^n$, where a larger score s_i indicates a greater deviation of node v_i from the normal patterns embedded in the incomplete graph \mathcal{G}_{obs} . During in-

ference, the problem is formulated as a ranking task, with higher scores marking as anomalies (Ding et al. 2019b).

2.3 Dual-pathway Incomplete Graph Imputation

Simultaneous incompleteness of node attributes and graph structure leads to mutual interference (Huo et al. 2023; Fu et al. 2023): attribute imputation relying on incomplete topology suffers from inaccurate neighborhood contexts, while structure completion based on incomplete or noisy attributes propagates reconstruction errors across the graph. To alleviate such interference, we propose a dual-pathway imputation module comprising: 1) a feature reconstruction pathway that imputes node attributes independently of structural information, and 2) a structure reconstruction pathway that enriches the observed sparse topology through global diffusion. The separately reconstructed attributes and structure are subsequently integrated to form a refined surrogate graph for improved downstream anomaly detection.

Feature Reconstruction Pathway To reconstruct missing node features, we employ a self-supervised MLP imputer. MLPs are robust to input sparsity and can flexibly model nonlinear relationships without relying on the graph topology (Yoon, Jordon, and van der Schaar 2018). Formally, given \mathbf{X}_{obs} and its binary mask \mathbf{M}_X , an MLP encoder f_θ is employed to reconstruct missing features as $\hat{\mathbf{X}} = f_\theta(\mathbf{X}_{\text{obs}})$, where f_θ is trained by minimizing the mean squared error (MSE) between observed entries in the original attribute matrix \mathbf{X} and their reconstructed $\hat{\mathbf{X}}$:

$$\mathcal{L}_{\text{feat}} = \text{MSE}(\mathbf{M}_X \odot \hat{\mathbf{X}}, \mathbf{M}_X \odot \mathbf{X}). \tag{1}$$

Structure Reconstruction Pathway To recover the incomplete graph topology, we adopt deterministic Personalized PageRank (PPR) diffusion (Park et al. 2019). This diffusion propagates relationships beyond immediate neighbors on a global scale, thus alleviating node isolation caused

by structural sparsity. Specifically, PPR iteratively diffuses structural information:

$$\mathbf{P}^{(t+1)} = \beta \,\tilde{\mathbf{A}} \,\mathbf{P}^{(t)} + (1 - \beta) \,\mathbf{I}, \qquad \tilde{\mathbf{A}} = \mathbf{A}_{\text{obs}} + \mathbf{I}, \quad (2)$$

where β is the teleport probability, and t represents the iteration step. After convergence at step T, the final diffused structure is obtained as $\mathbf{A}_{ppr} = \mathbf{P}^T$. The enhanced adjacency is then obtained by superimposing the diffusion result on the original observation:

$$\hat{\mathbf{A}} = \mathbf{A}_{\text{obs}} + \mathbf{A}_{\text{ppr}}.\tag{3}$$

The pair $(\hat{\mathbf{A}}, \hat{\mathbf{X}})$ constitutes a densified surrogate graph used in the subsequent anomaly-scoring module.

2.4 Joint Latent-Space Modeling

While the dual-pathway imputer reduces cross interference, it ignores the intrinsic co-dependencies between attributes and structure, i.e., a missing node feature can be inferred from the attributes of its neighbors, and conversely, a missing edge may be recovered using similarity in node features. To capture these dependencies, we embed both reconstructed views into a shared latent space, allowing each view to mutually refine and complement the other. Then we impose 1) a spherical prior to compact normal nodes and 2) a reconstruction objective to preserve fine-grained semantics.

Latent-Space Fusion and Spherical Constraint Formally, we denote the GCN projector by g_{γ} , an L-layer GCN with propagation rules:

$$\mathbf{Z}^{(0)} = \hat{\mathbf{X}}, \quad \mathbf{Z}^{(l)} = \sigma(\hat{\mathbf{A}} \, \mathbf{Z}^{(l-1)} \, W^{(l)}) \quad (l = 1, \dots, L),$$

where $W^{(l)} \in \mathbb{R}^{d_{l-1} \times d_l}$ and $\sigma(\cdot)$ is ReLU. The fused node embedding is then simply $\mathbf{Z} = g_{\gamma}(\hat{\mathbf{X}}, \hat{\mathbf{A}}) = \mathbf{Z}^{(L)}$.

To shape the empirical distribution of \mathbf{Z} , a Sinkhorn divergence $\mathcal{L}_{\text{dist}}$ is minimised between \mathbf{Z} and a truncated Gaussian prior $\mathcal{N}_r(\mathbf{0}, \mathbf{I})$ supported on the latent ball $||z||_2 \leq r$:

$$\mathcal{L}_{\text{dist}} = \text{Sinkhorn}(\mathbf{Z}, \mathcal{N}_r(\mathbf{0}, \mathbf{I})).$$
 (4)

Under the assumption that most nodes are normal, this constraint compacts their embeddings within radius r and implicitly reserves the exterior for anomalies. Unlike point-to-center objectives (e.g., SVDD (Ruff et al. 2018)), Sinkhorn offers global distribution matching: it aligns the entire embedding cloud to the truncated-Gaussian prior, encouraging a meaningful spread of normal patterns inside the latent ball and preventing trivial collapse.

Latent Semantics Preservation via Reconstruction To tether the compact latent space to the input's fine-grained semantics, we append a two-layer MLP recovery decoder r_{ω} seeking to reconstruct node attributes from the embeddings, i.e., $\tilde{\mathbf{X}} = r_{\omega}(\mathbf{Z})$, trained under the MSE objective:

$$\mathcal{L}_{\text{recon}} = \text{MSE}(\mathbf{M}_X \odot \tilde{\mathbf{X}}, \mathbf{M}_X \odot \mathbf{X}). \tag{5}$$

Jointly minimising $\mathcal{L}_{\mathrm{recon}}$ alongside the spherical Sinkhorn loss preserves attribute–structure details in each embedding for faithful reconstruction and prevents collapse.

2.5 Graph Pseudo-Anomaly Generation

The scarcity of true anomalies and the absence of labels can cause imputation bias: a model trained almost exclusively on majority-normal data tends to reconstruct anomalous nodes as if they were normal, thereby erasing distinctive signals and degrading detection performance. To counteract this effect we aim to generate sufficient pseudo-anomalies. The idea is to sample latent codes that lie just outside the compact normal region, decode them into node attributes via the decoder r_{ω} , endow them with a lightweight internal topology, and append the resulting subgraph to the training graph as hard negative examples.

Latent-Space Sampling After the latent-space training in Section 2.4, normal embeddings are concentrated inside a ball of radius r. Rather than sampling latent codes arbitrarily far from this region, which can produce trivial or unrealistic outliers, we focus on the margin where boundary refinement is most critical. Specifically, we sample M latent vectors $\{\mathbf{z}_i^{(a)}\}_{i=1}^M$ uniformly from an annular shell:

$$S_{\text{shell}} = \{ \mathbf{z} \in \mathbb{R}^{d_z} \mid r_a < \|\mathbf{z}\|_2 < r_b \}. \tag{6}$$

Vectors in this shell remain close enough to the normal manifold to be decoded into realistic feature–structure patterns, yet lie just outside the compact region, providing hard negative examples that sharpen the model's decision boundary. To avoid excessive hyper-parameter tuning, we set $r_a=1.2\,r$ and $r_b=2r$ for all experiments, which we find to work robustly across datasets.

Synthetic Graph Construction Each sampled vector is then mapped to the original attribute space through the decoder, i.e., $\tilde{x}^{(a)} = r_{\omega}(z_i^{(a)})$. Since the decoder has been trained to reconstruct authentic node features, the resulting $\tilde{x}_i^{(a)}$ resembles plausible but atypical nodes.

However, a key challenge is how to embed the pseudoanomaly nodes into the training graph, without introducing spurious connections that would either corrupt the normal manifold, or yield unrealistic, uninformative structures (e.g., if left isolated). To address this, we create an internal pseudo-anomaly subgraph whose edges reflect feature similarity, while keeping it disconnected from the real nodes.

Specifically, we compute pairwise cosine similarity among the decoded features and connect node pair (i,j) whenever $\cos(\tilde{x}_i^{(a)},\tilde{x}_j^{(a)}) \geq \tau_a$, yielding an adjacency matrix $\mathbf{S}^{(a)} \in (0,1)^{M \times M}$. To align with the characteristics of \mathbf{A}_{obs} , we perform row-wise min-max normalization on $\mathbf{S}^{(a)}$, followed by binarization with a fixed threshold $\tau_a = 0.5$:

$$\mathbf{A}_{ij}^{(a)} = \mathbb{I}\left(\frac{\mathbf{S}_{ij}^{(a)} - \min_{k} \mathbf{S}_{ik}^{(a)}}{\max_{k} \mathbf{S}_{ik}^{(a)} - \min_{k} \mathbf{S}_{ik}^{(a)}} \ge \tau_{a}\right). \tag{7}$$

This ensures all node-specific similarities are mapped to [0,1], preserving local topological rankings while enabling direct comparison with \mathbf{A}_{obs} .

Finally, we build a block-diagonal augmented graph:

$$\mathbf{A}_{\mathrm{aug}} = \begin{bmatrix} \mathbf{A}_{\mathrm{obs}} & \mathbf{0} \\ \mathbf{0} & \mathbf{A}^{(a)} \end{bmatrix}, \qquad \mathbf{X}_{\mathrm{aug}} = \begin{bmatrix} \mathbf{X}_{\mathrm{obs}} \\ \tilde{\mathbf{X}}^{(a)} \end{bmatrix}.$$
 (8)

DI Method	GAD Method	Cora	Citeseer	Books	Disney	Flickr	ACM	Reddit
	COLA (TNNLS 2022) (Liu et al. 2022)	0.46 ± 0.02	0.44 ± 0.02	0.50 ± 0.04	0.48 ± 0.09	0.50 ± 0.01	0.45 ± 0.01	0.51 ± 0.02
	PREM (ICDM 2023) (Pan et al. 2023)	0.63 ± 0.02	0.67 ± 0.01	0.36 ± 0.02	0.29 ± 0.07	0.58 ± 0.01	0.59 ± 0.01	0.54 ± 0.01
Mean	GRADATE (AAAI 2023) (Duan et al. 2023)	0.49 ± 0.03	0.48 ± 0.02	0.52 ± 0.08	0.49 ± 0.09	0.46 ± 0.02	0.46 ± 0.05	0.51 ± 0.05
	ADA-GAD (AAAI 2024) (He et al. 2024)	0.84 ± 0.01	0.90 ± 0.01	0.41 ± 0.05	0.40 ± 0.04	0.70 ± 0.01	0.78 ± 0.00	0.56 ± 0.01
	DiffGAD (ICLR 2025) (Li et al. 2025)	0.52 ± 0.05	0.50 ± 0.08	0.51 ± 0.07	0.49 ± 0.06	0.51 ± 0.01	0.60 ± 0.01	0.52 ± 0.05
	COLA (TNNLS 2022) (Liu et al. 2022)	0.52 ± 0.01	0.49 ± 0.02	0.49 ± 0.10	0.55 ± 0.12	0.64 ± 0.01	0.48 ± 0.02	0.52 ± 0.01
MissForest	PREM (ICDM 2023) (Pan et al. 2023)	0.65 ± 0.01	0.65 ± 0.01	0.40 ± 0.04	0.37 ± 0.08	0.75 ± 0.01	0.66 ± 0.01	0.55 ± 0.00
	GRADATE (AAAI 2023) (Duan et al. 2023)	0.52 ± 0.03	0.49 ± 0.01	0.54 ± 0.10	$0.55{\pm}0.05$	0.64 ± 0.01	0.48 ± 0.07	0.55 ± 0.03
	ADA-GAD (AAAI 2024) (He et al. 2024)	0.84 ± 0.01	0.70 ± 0.13	0.54 ± 0.12	0.45 ± 0.06	0.69 ± 0.01	0.78 ± 0.01	0.49 ± 0.05
	DiffGAD (ICLR 2025) (Li et al. 2025)	0.50 ± 0.10	0.55 ± 0.03	0.48 ± 0.05	0.45 ± 0.10	0.62 ± 0.01	0.48 ± 0.01	0.48 ± 0.04
	COLA (TNNLS 2022) (Liu et al. 2022)	0.53 ± 0.04	0.53 ± 0.01	0.52 ± 0.06	0.58 ± 0.11	0.48 ± 0.03	0.51 ± 0.01	0.50 ± 0.02
GAE	PREM (ICDM 2023) (Pan et al. 2023)	0.41 ± 0.08	0.32 ± 0.02	0.40 ± 0.04	0.46 ± 0.13	0.55 ± 0.02	0.48 ± 0.06	0.51 ± 0.01
	GRADATE (AAAI 2023) (Duan et al. 2023)	0.49 ± 0.02	0.50 ± 0.02	0.58 ± 0.05	0.55 ± 0.17	0.49 ± 0.01	0.50 ± 0.02	0.49 ± 0.03
	ADA-GAD (AAAI 2024) (He et al. 2024)	0.66 ± 0.02	0.64 ± 0.04	0.57 ± 0.09	0.51 ± 0.11	0.56 ± 0.01	0.64 ± 0.01	0.55 ± 0.01
	DiffGAD (ICLR 2025) (Li et al. 2025)	0.66 ± 0.02	0.61 ± 0.01	0.49 ± 0.03	0.46 ± 0.08	0.61 ± 0.01	0.57 ± 0.01	0.51 ± 0.06
	COLA (TNNLS 2022) (Liu et al. 2022)	0.54 ± 0.02	0.49 ± 0.03	0.66 ± 0.01	0.54 ± 0.01	0.37 ± 0.11	0.53 ± 0.05	0.50 ± 0.02
	PREM (ICDM 2023) (Pan et al. 2023)	0.64 ± 0.00	0.66 ± 0.02	0.58 ± 0.04	0.59 ± 0.01	$0.35{\pm}0.05$	0.40 ± 0.03	0.56 ± 0.01
ASD-VAE	GRADATE (AAAI 2023) (Duan et al. 2023)	0.51 ± 0.03	0.49 ± 0.03	0.58 ± 0.03	0.51 ± 0.05	0.39 ± 0.22	0.49 ± 0.06	0.49 ± 0.01
	ADA-GAD (AAAI 2024) (He et al. 2024)	0.83 ± 0.01	0.90 ± 0.01	0.70 ± 0.00	0.78 ± 0.01	0.41 ± 0.09	0.43 ± 0.06	0.56 ± 0.00
	DiffGAD (ICLR 2025) (Li et al. 2025)	0.79 ± 0.01	0.50 ± 0.00	0.50 ± 0.00	0.50 ± 0.00	0.48 ± 0.08	0.50 ± 0.00	0.55 ± 0.00
	COLA (TNNLS 2022) (Liu et al. 2022)	0.53 ± 0.01	0.50 ± 0.03	0.50 ± 0.08	0.58 ± 0.10	0.67 ± 0.01	0.56 ± 0.01	0.51 ± 0.02
	PREM (ICDM 2023) (Pan et al. 2023)	0.62 ± 0.02	0.66 ± 0.01	0.42 ± 0.02	0.61 ± 0.06	0.56 ± 0.04	0.57 ± 0.01	0.55 ± 0.01
GAIN	GRADATE (AAAI 2023) (Duan et al. 2023)	0.49 ± 0.03	0.51 ± 0.05	0.58 ± 0.08	0.57 ± 0.07	0.61 ± 0.03	0.52 ± 0.03	0.53 ± 0.04
	ADA-GAD (AAAI 2024) (He et al. 2024)	0.84 ± 0.01	0.90 ± 0.01	0.60 ± 0.04	$0.44{\pm}0.12$	0.74 ± 0.01	0.82 ± 0.01	0.47 ± 0.01
	DiffGAD (ICLR 2025) (Li et al. 2025)	0.47 ± 0.08	0.50 ± 0.01	0.51 ± 0.01	$0.46 {\pm} 0.07$	0.65 ± 0.01	0.53 ± 0.01	0.49 ± 0.04
	M ² V-UGAD (ours)	0.93±0.02	$0.92 {\pm} 0.02$	0.63 ± 0.02	$0.81 {\pm} 0.05$	$0.93{\pm}0.01$	$0.92 {\pm} 0.01$	$0.58 {\pm} 0.02$

Table 1: Detection performance comparison with the existing GAD methods under 30% missing rate in terms of AUROC.

The synthetic subgraph thus supplies realistic, self-contained pseudo-anomalies that act as explicit contrastive signals, sharpening the decision boundary of the downstream anomaly detector without introducing spurious mixed-type edges.

2.6 Training Pipeline and Anomaly Scoring

Overall, our training proceeds in two stages. In the pre-training stage, we jointly optimize $\mathcal{L}_{\mathrm{pretrain}}$ on the original graph $(\mathbf{X}_{\mathrm{obs}}, \mathbf{A}_{\mathrm{obs}})$:

$$\mathcal{L}_{pretrain} = \mathcal{L}_{dist} + \alpha \mathcal{L}_{feat} + \lambda \mathcal{L}_{recon}, \qquad (9)$$

where α,λ are hyperparameters balancing their contributions. In the fine-tuning stage, we augment the data with $M=\eta n$ pseudo-anomalies (η denotes the fraction of pseudo-anomaly nodes among all training samples), to obtain ($\mathbf{X}_{\mathrm{aug}},\mathbf{A}_{\mathrm{aug}}$) and re-optimise:

$$\mathcal{L}_{\text{finetune}} = \mathcal{L}'_{\text{dist}} + \alpha \mathcal{L}_{\text{feat}} + \lambda \mathcal{L}_{\text{recon}},$$
 (10)

where

$$\mathcal{L}'_{\text{dist}} = \text{Sinkhorn}(\mathbf{Z}_{\text{pseudo}}, \mathcal{N}_{\{r_a < ||z||_2 \le r_b\}}(0, \mathbf{I})) + \text{Sinkhorn}(\mathbf{Z}, \mathcal{N}_r(0, \mathbf{I}))$$
(11)

compacts normal embeddings inside the radius r ball while pushing pseudo-anomaly embeddings toward the outer shell $\{r_a < \|z\|_2 \le r_b\}$. During inference, each node v_i is processed through the trained imputers and projector to produce its latent embedding z_i . Its anomaly score is defined as $s_i = \|z_i\|_2$, where larger values indicate greater deviation from the learned normal region.

3 Experiment

3.1 Datasets

We perform experiments on seven real-world attributed graphs spanning diverse application domains. Four of these datasets (Cora, Citeseer, Flickr, and ACM) do not include ground-truth anomaly labels and are hence used for anomaly injection, while the other three (Books, Disney, and Reddit) contain inherent anomalies derived from user behavior or content semantics. For the injection datasets, we follow the CoLA protocol (Liu et al. 2022) to synthesize structural anomalies by randomly rewiring edges among a subset of nodes and contextual anomalies by replacing selected nodes' feature vectors with those of semantically distant peers. To simulate real-world missingness, we randomly mask 30% of nodes and 30% of edges in every graph for our main experiments; Table 2 explores additional masking rates to evaluate the robustness of our method under varying degrees of incompleteness. The summary statistics of all datasets are presented in the Supplementary Material.

3.2 Baseline Methods and Implementation Details

We compare M²V-UGAD against five recent unsupervised GAD models, including CoLA (Liu et al. 2022), PREM (Pan et al. 2023), GRADATE (Duan et al. 2023), ADA-GAD (He et al. 2024), and DiffGAD (Li et al. 2025). None of these detectors natively supports graphs with missing nodes or edges; therefore, we adopt a two-stage "impute-then-detect" pipeline. In the first stage, we restore missing values using one of five data imputation (DI) methods (Mean Filling, MissForest (Stekhoven and Bühlmann 2011), GAIN (Yoon, Jordon, and van der Schaar 2018), GAE (Kipf and Welling 2016), or ASD-VAE (Jiang et al. 2024)). In the second stage, we apply each detector to each imputed graph. All methods

Dataset	DI Method	GAD Method	10%	20%	30%	40%	50%
	Mean	COLA (TNNLS 2022) (Liu et al. 2022)	0.53 ± 0.02	0.49 ± 0.02	0.46 ± 0.02	0.44 ± 0.01	0.47 ± 0.02
		PREM (ICDM 2023) (Pan et al. 2023)	0.70 ± 0.01	0.66 ± 0.02	0.63 ± 0.02	0.62 ± 0.02	0.65 ± 0.01
		GRADATE (AAAI 2023) (Duan et al. 2023)	0.50 ± 0.04	0.52 ± 0.02	0.49 ± 0.03	0.49 ± 0.02	0.49 ± 0.02
		ADA-GAD (AAAI 2024) (He et al. 2024)	0.85 ± 0.01	0.85 ± 0.00	0.84 ± 0.01	0.82 ± 0.01	0.82 ± 0.01
		DiffGAD (ICLR 2025) (Li et al. 2025)	0.53 ± 0.06	0.47 ± 0.01	0.52 ± 0.05	0.53 ± 0.08	0.46 ± 0.08
	MissForest	COLA (TNNLS 2022) (Liu et al. 2022)	0.53 ± 0.01	0.56 ± 0.01	0.52 ± 0.01	0.53 ± 0.01	0.55 ± 0.01
		PREM (ICDM 2023) (Pan et al. 2023)	0.71 ± 0.01	0.70 ± 0.01	0.65 ± 0.01	0.64 ± 0.00	0.64 ± 0.01
		GRADATE (AAAI 2023) (Duan et al. 2023)	0.52 ± 0.02	0.48 ± 0.01	0.52 ± 0.03	0.52 ± 0.03	0.53 ± 0.02
		ADA-GAD (AAAI 2024) (He et al. 2024)	0.86 ± 0.01	0.85 ± 0.01	0.84 ± 0.01	0.80 ± 0.00	0.77 ± 0.01
		DiffGAD (ICLR 2025) (Li et al. 2025)	0.45 ± 0.07	0.51 ± 0.07	0.50 ± 0.10	0.53 ± 0.10	0.49 ± 0.09
	GAE	COLA (TNNLS 2022) (Liu et al. 2022)	0.52 ± 0.02	0.53 ± 0.04	0.53 ± 0.04	0.56 ± 0.01	0.51 ± 0.02
		PREM (ICDM 2023) (Pan et al. 2023)	0.39 ± 0.06	0.32 ± 0.03	0.41 ± 0.08	0.40 ± 0.06	0.35 ± 0.06
Cora		GRADATE (AAAI 2023) (Duan et al. 2023)	0.52 ± 0.02	0.51 ± 0.02	0.49 ± 0.02	0.52 ± 0.04	0.47 ± 0.03
Cora		ADA-GAD (AAAI 2024) (He et al. 2024)	0.67 ± 0.01	0.65 ± 0.01	0.66 ± 0.02	0.60 ± 0.02	0.58 ± 0.01
		DiffGAD (ICLR 2025) (Li et al. 2025)	0.68 ± 0.02	0.66 ± 0.02	0.66 ± 0.02	0.59 ± 0.01	0.64 ± 0.01
	ASD-VAE	COLA (TNNLS 2022) (Liu et al. 2022)	0.51 ± 0.02	0.52 ± 0.02	0.54 ± 0.02	0.52 ± 0.00	0.55 ± 0.01
		PREM (ICDM 2023) (Pan et al. 2023)	0.69 ± 0.01	0.66 ± 0.01	0.64 ± 0.00	0.63 ± 0.03	0.60 ± 0.02
		GRADATE (AAAI 2023) (Duan et al. 2023)	0.50 ± 0.03	0.51 ± 0.01	0.51 ± 0.03	0.52 ± 0.03	0.50 ± 0.02
		ADA-GAD (AAAI 2024) (He et al. 2024)	0.86 ± 0.01	0.84 ± 0.01	0.83 ± 0.01	0.83 ± 0.01	0.82 ± 0.01
		DiffGAD (ICLR 2025) (Li et al. 2025)	0.78 ± 0.02	0.79 ± 0.01	0.79 ± 0.01	0.50 ± 0.01	0.50 ± 0.01
	GAIN	COLA (TNNLS 2022) (Liu et al. 2022)	0.54 ± 0.02	0.53 ± 0.01	0.53 ± 0.01	0.55 ± 0.02	0.57 ± 0.04
		PREM (ICDM 2023) (Pan et al. 2023)	0.69 ± 0.01	0.64 ± 0.01	0.62 ± 0.02	0.58 ± 0.02	0.63 ± 0.01
		GRADATE (AAAI 2023) (Duan et al. 2023)	0.51 ± 0.03	0.50 ± 0.03	0.49 ± 0.03	0.50 ± 0.01	0.53 ± 0.02
		ADA-GAD (AAAI 2024) (He et al. 2024)	0.86 ± 0.01	0.84 ± 0.01	0.84 ± 0.01	0.83 ± 0.00	0.83 ± 0.01
		DiffGAD (ICLR 2025) (Li et al. 2025)	0.55 ± 0.07	0.60 ± 0.09	0.47 ± 0.08	0.51 ± 0.06	0.50 ± 0.01
		M ² V-UGAD (ours)	0.93 ± 0.01	0.93 ± 0.02	0.93 ± 0.02	0.92 ± 0.01	0.92 ± 0.01

Table 2: Detection performance comparison with the existing GAD methods under various missing rates in terms of AUROC.

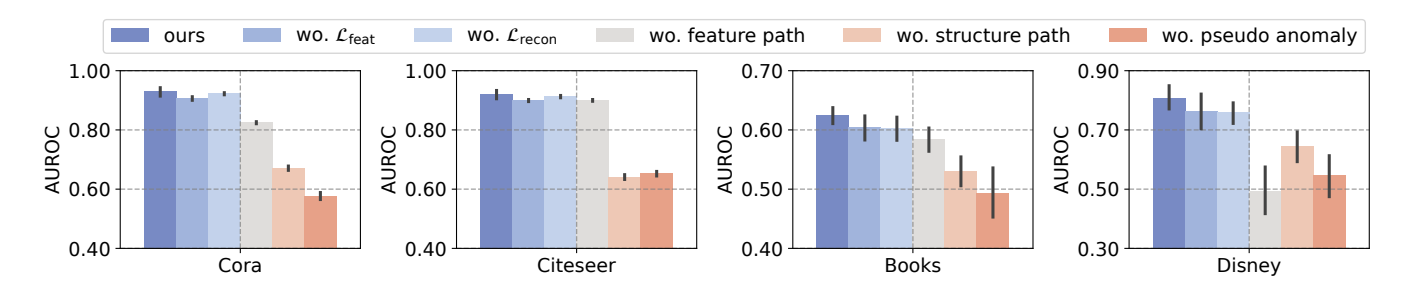


Figure 2: Ablation experiments of M²V-UGAD under 30% missing rate in terms of AUROC.

are evaluated using the Area Under the ROC Curve (AU-ROC) with performance averaged over 5 independent runs. Detailed descriptions of each detector, imputer, pairing protocol, and the full M²V-UGAD configuration are provided in the Supplementary Material.

3.3 Comparison Study

Table 1 summarizes the AUROC scores for all methods across seven datasets at a 30% missingness, while Table 2 further reports performance on the Cora dataset with varying masking ratios. Overall, M²V-UGAD consistently outperforms all baselines across diverse experimental setups and the majority of datasets.

The suboptimal performance of the baselines stems from the limitations of the imputation methods. Mean Filling, MissForest, and GAIN treat nodes independently and neglect the structural relationships among nodes, resulting in large imputation errors under severe incompleteness. While GAE and ASD-VAE leverage graph topology, they implicitly assume that the observed structural information is complete and reliable. When edges are also missing, structural

noise adversely affects attribute imputation due to mutual interference between structure and node attributes. Incomplete edges can further disrupt standard message-passing mechanisms. Even for low imputation error, the predominance of normal nodes introduces imputation bias, diluting the distinctive signals required for accurate anomaly detection.

Subsequent anomaly detectors can amplify errors or biases introduced during imputation. Contrastive learning methods like CoLA and PREM, detect anomalies based on discrepancies between nodes and their local or global neighborhoods. If imputation errors are large, these methods can inaccurately represent normal node characteristics. Conversely, strong imputation bias can homogenize reconstructed node attributes, blurring distinctions between anomalous and normal nodes. ADA-GAD can partially mitigate imputation errors through its anomaly-denoised pretraining strategy, which is evidenced by its higher performance in comparison to other baselines. However, its finetuning step is conducted on the fully imputed graph, making it difficult to rescue anomalies that have already been smoothed into normal patterns.

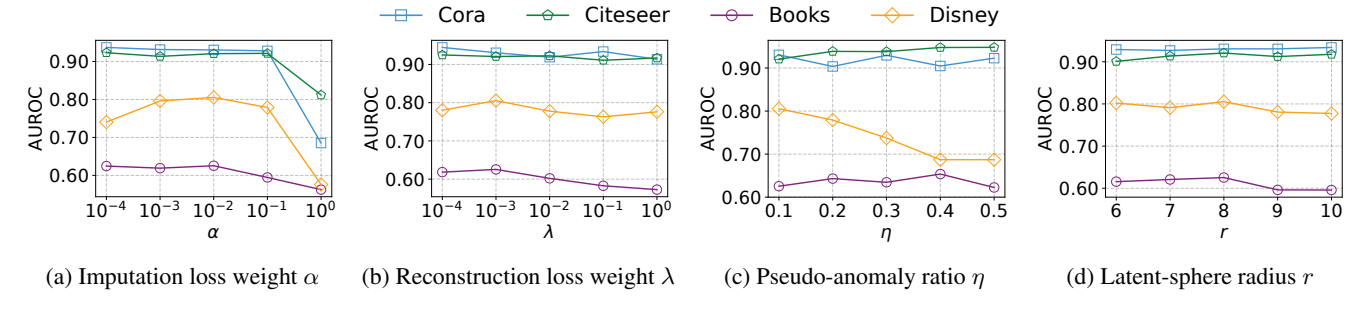


Figure 3: Sensitivity analysis of M²V-UGAD under 30% missing rate in terms of AUROC.

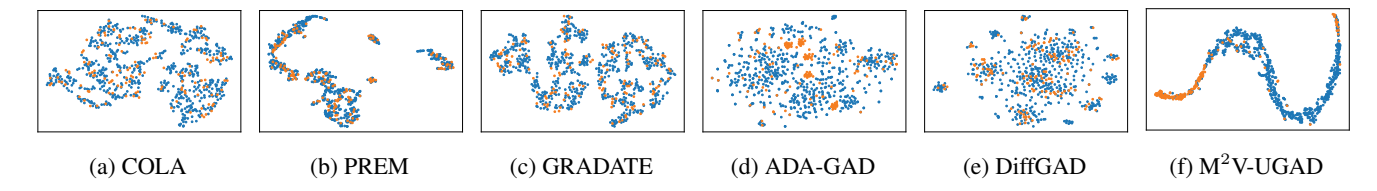


Figure 4: t-SNE embedding of various GAD methods (with GAIN as DI) and M²V-UGAD on Cora under 30% missing rate.

3.4 Ablation Study

We systematically ablate the main building blocks of M²V-UGAD on Cora, Citeseer, Books, and Disney with 30% missingness to gauge their individual impact (Figure 2). Removing either the $\mathcal{L}_{\mathrm{feat}}$ imputation loss or the $\mathcal{L}_{\mathrm{recon}}$ reconstruction loss produces a moderate AUROC decline $(\approx 2-4\%$ on most datasets), confirming that both objectives are needed to enhance imputation fidelity and maintain a well-behaved latent manifold. Eliminating an entire pathway is more damaging: dropping the feature-imputation branch lowers AUROC by roughly 3% to 10%, while discarding the structure-reconstruction path yields the steepest degradation among the two (\approx 10-30%). These underscore the importance of the dual-path design in preventing cross-view contamination. The most pronounced impact arises when the pseudo-anomaly generation process is disabled, slashing AUROC by roughly 10% to 35% across all datasets. This highlights its crucial role in countering imputation bias and sharpening the decision boundary. Collectively, these results verify that each component of M²V-UGAD is indispensable for robust anomaly detection on incomplete graphs.

3.5 Sensitivity Analysis

We conduct a comprehensive sensitivity study to examine how four key hyper-parameters affect the performance of M²V-UGAD under the default 30% missingness (Figure 3). For the imputation loss weight α , AUROC peaks when α lies in the corridor $0.001 \leq \alpha \leq 0.01$; Setting α to a low number like 0.0001 may under-train the feature imputer, which is evidenced by a slight drop on Disney. Whereas setting $\alpha>0.01$ shifts optimisation away from the latent objectives and leads to a clear decline on all datasets. For the reconstruction loss weight λ , raising λ from 0.001 to 1 induces a monotonic yet mild downward trend, while a small dip also appears at 0.0001. These observations suggest that

extremely small λ weakens latent semantics, whereas overly large values over-regularise and blunt anomaly separation, although overall performance remains stable across roughly two orders of magnitude. In terms of the pseudo-anomaly ratio η , most datasets are almost insensitive to variations within $0.1 \le \eta \le 0.5$; While Disney exhibits a gradual decline as η grows. This is likely because an excessive synthetic set can dilute the decision boundary on very small graphs. Hence a moderate ratio $(\eta - 0.1 \sim 0.3)$ offers a sound trade-off. Finally, adjusting the latent-sphere radius rbetween 6 and 8 leaves AUROC virtually unchanged, and expanding it to 10 induces only a mild decrease (below two percentage points) on Books and Disney, indicating that the Sinkhorn alignment adapts robustly provided r is not extreme. Overall, the results suggest that M²V-UGAD is relatively less sensitive to various parameter settings.

3.6 Visualization Study

Figure 4 shows the node embeddings from M²V-UGAD alongside five GAD methods using GAIN for data imputation, on the Cora dataset with 30% attribute and structural missingness. For the five baselines (Figure 4a-4e), anomalies (orange points) are clearly entangled with normal nodes (blue points), leading to blurred boundaries and difficulty in anomaly discrimination. In contrast, embeddings produced by M²V-UGAD (Figure 4f) exhibit a clear distinction, where normal nodes are arranged along a smooth manifold, while anomalous nodes are predominantly positioned on the periphery, clearly separated from the main distribution of normal nodes. This stark contrast highlights the superior ability of our proposed components, including the dual-pathway imputation, spherical latent alignment, and pseudo-anomaly generation, to preserve and emphasize anomaly signals under significant attribute and structure missingness.

Dataset	Node	Edge	Feature	Average Degree	Outliers	Outlier Ratio
Cora	2,708	5,803	1,433	4.3	150	5.54%
Citeseer	3,327	5,137	3,703	3.1	150	4.51%
Books	1,418	1,847	21	2.6	28	1.97%
Disney	124	167	28	2.7	6	4.84%
Flickr	7,575	241,304	12,047	63.7	450	5.94%
ACM	16,484	82,175	8,337	10	597	3.62%
Reddit	10,984	84,008	64	15.3	366	3.33%

Table 3: Statistics of datasets adopted in the experiments.

4 Conclusion

In this paper, we present the first investigation into unsupervised graph anomaly detection under simultaneous incompleteness of node attributes and graph topology. We propose M²V-UGAD, a framework combining dual-pathway imputation, Sinkhorn-driven latent regularization, and pseudoanomaly synthesis to address feature–structure interference and imputation bias. Extensive experiments verify the effectiveness of each component and demonstrate that M²V-UGAD significantly outperforms a variety of existing graph anomaly detection methods coupled with different imputation strategies across multiple benchmark datasets.

5 Appendix

5.1 Baselines and Evaluation Metric

We benchmark five state-of-the-art unsupervised graph anomaly detection methods: 1) CoLA (Liu et al. 2022), which employs a local–global contrastive learning approach and trains a discriminator to identify inconsistencies between a node and its neighborhood; 2) PREM (Pan et al. 2023), which detects anomalies by directly measuring ego–neighbor similarity without message passing; 3) GRA-DATE (Duan et al. 2023), which utilizes multi-scale contrastive learning with dual graph views to capture both local and global irregularities; 4) ADA-GAD (He et al. 2024), which adopts a two-stage denoise-then-detect pipeline with anomaly-aware regularization; and 5) DiffGAD (Li et al. 2025), which leverages diffusion models to score anomalies in the latent space.

Since none of these detectors natively handles graphs with missing nodes or edges, we adopt a two-stage "impute-then-detect" strategy. First, we complete the graphs using one of five general-purpose imputers—mean filling (column-wise averages), MissForest (Stekhoven and Bühlmann 2011), GAIN (Yoon, Jordon, and van der Schaar 2018), GAE (Kipf and Welling 2016), or ASD-VAE (Jiang et al. 2024). The first three methods ignore graph topology and impute only node features, whereas GAE and ASD-VAE leverage the observed topology to guide feature reconstruction. Second, we apply each of the five detectors to each of the five imputed graphs, yielding 25 impute-then-detect baseline combinations.

For evaluation, we use the Area Under the Receiver Operating Characteristic curve (AUROC) as our primary evaluation metric. AUROC provides a threshold-independent measure of the model's ability to distinguish between normal

and anomalous nodes, and is widely adopted for anomaly detection due to its robustness to class imbalance.

5.2 Model Configuration

All experiments are conducted on a single NVIDIA A100 GPU (40 GB memory) using PyTorch 2.2 and PyG 2.5. We train using the Adam optimizer, with the learning rate selected from the set $\{0.0001, 0.001, 0.0005\}$ according to the speed of training loss convergence. Both initial training and fine-tuning phases are run for 100 epochs each. The latent dimension d_z is set to 256 for most datasets, except for Flickr and ACM, where it is reduced to 128 due to memory constraints. We use a two-layer GCN encoder in all experiments. The Sinkhorn divergence uses regularization $\epsilon=0.1$ with 1000 iterations. For pseudo-anomaly generation, we sample M=0.1n latent vectors, corresponding to 10% of the training nodes. Loss component weights (α,λ) are selected from $\{0.1,0.01,0.001,0.0001\}$ based on the training loss, and we fix them at $\alpha=0.01$ and $\lambda=0.001$ for all datasets.

5.3 Datasets

We perform experiments on seven real-world attributed graphs spanning diverse application domains, including Cora (Yang, Cohen, and Salakhudinov 2016), Citeseer (Yang, Cohen, and Salakhudinov 2016), Flickr (Zeng et al. 2020), and ACM (Tang et al. 2008), Disney (Müller et al. 2013), Books (Sánchez et al. 2013), and Reddit (Kumar, Zhang, and Leskovec 2019). Table 3 summarizes each graph's number of nodes, number of edges, feature dimensionality, average node degree, number of anomalous nodes and anomaly ratio.

5.4 Pseudo code

See Algorithm 1

Acknowledgements

This work was supported in part by the National Natural Science Foundation of China under Grant 62262005, in part by the High-level Innovative Talents in Guizhou Province under Grant GCC[2023]033, in part by the Open Project of the Text Computing and Cognitive Intelligence Ministry of Education Engineering Research Center under Grant TCCI250208.

Algorithm 1: M²V-UGAD Training and Inference

```
1: Input: incomplete graph (\mathcal{V}, \mathbf{X}_{\text{obs}}, \mathbf{A}_{\text{obs}}, \mathbf{M}_X, \mathbf{M}_A);
          hyperparameters \alpha, \lambda, r, r_a, r_b, \eta; epochs T_{\text{pre}}, T_{\text{fine}}
  2: Output: anomaly scores \{s_i\}_{i=1}^{|\mathcal{V}|}
   3: 1. Dual-pathway imputation
   4:
                X \leftarrow f_{\theta}(X_{\text{obs}}) {Feature path}
                \hat{A} \leftarrow A_{\text{obs}} + \text{PPR}(A_{\text{obs}}) \{ \text{Structure path} \}
   5:
   6: 2. Pre-training
  7: for t=1 to T_{\rm pre} do
                \mathbf{Z} \leftarrow g_{\gamma}(\hat{\mathbf{X}}, \hat{\mathbf{A}})
   8:
               \tilde{\mathbf{X}} \leftarrow r_{\omega}(\mathbf{Z})
  9:
                \mathcal{L}_{\text{feat}} \leftarrow \text{MSE}(\mathbf{M}_X \odot \hat{\mathbf{X}}, \, \mathbf{M}_X \odot \mathbf{X}_{\text{obs}})
10:
                \mathcal{L}_{\text{dist}} \leftarrow \text{Sinkhorn}(\mathbf{Z}, \mathcal{N}_r(0, I))
11:
12:
                \mathcal{L}_{\text{recon}} \leftarrow \text{MSE}(\mathbf{M}_X \odot \tilde{\mathbf{X}}, \, \mathbf{M}_X \odot \mathbf{X}_{\text{obs}})
13:
                \mathcal{L}_{pre} \leftarrow \alpha \mathcal{L}_{feat} + \mathcal{L}_{dist} + \lambda \mathcal{L}_{recon}
                Update \{\theta, \gamma, \omega\} by gradient descent on \mathcal{L}_{pre}
14:
15: end for
16: 3. Pseudo-anomaly generation
                M \leftarrow |\eta|\mathcal{V}| {number of pseudo nodes}
17:
               Sample \{z_i^{(a)}\}_{i=1}^M from \{z: r_a < \|z\|_2 < r_b\}
18:
               \tilde{\mathbf{X}}^{(a)} \leftarrow r_{\omega}(\{z_i^{(a)}\})
19:
               \mathbf{A}^{(a)} \leftarrow \mathrm{SimilarityThreshold}(\tilde{X}^{(a)}, \tau_a = 0.5)
20:
               \mathbf{X}_{\mathrm{aug}} \leftarrow [\mathbf{X}_{\mathrm{obs}}; \mathbf{X}^{(a)}], \quad \mathbf{A}_{\mathrm{aug}} \leftarrow \begin{bmatrix} \mathbf{A}_{\mathrm{obs}} & 0 \\ 0 & \mathbf{A}^{(a)} \end{bmatrix}
21:
22: 4. Fine-tuning
23: for t=1 to T_{\mathrm{fine}} do
               \begin{aligned} &\mathbf{Z}_{\text{aug}} \leftarrow g_{\gamma}(\hat{\mathbf{X}}_{\text{aug}}, \hat{\mathbf{A}}_{\text{aug}}) \\ &\text{Split } \mathbf{Z}_{\text{aug}} \text{ into } (\mathbf{Z}, \mathbf{Z}_{\text{pseudo}}) \\ &\mathcal{L}'_{\text{dist}} \leftarrow &\text{SINKHORN}(\mathbf{Z}, \mathcal{N}_r) \\ &\text{SINKHORN}(\mathbf{Z}_{\text{pseudo}}, \mathcal{N}_{\{r_a < \|z\| \le r_b\}}) \end{aligned}
24:
25:
26:
                \mathbf{X}_{\mathrm{aug}} \leftarrow r_{\omega}(\mathbf{Z}_{\mathrm{aug}})
27:
                \mathcal{L}_{\text{feat}} \leftarrow \text{MSE}(\mathbf{M}_X \odot \hat{\mathbf{X}}_{\text{aug}}, \, \mathbf{M}_X \odot \mathbf{X}_{\text{aug}})
28:
                \mathcal{L}_{\text{recon}} \leftarrow \text{MSE}(\mathbf{M}_X \odot \tilde{\mathbf{X}}_{\text{aug}}, \, \mathbf{M}_X \odot \mathbf{X}_{\text{aug}})
29:
                \mathcal{L}_{\text{finetune}} \leftarrow \alpha \mathcal{L}_{\text{feat}} + \mathcal{L}'_{\text{dist}} + \lambda \mathcal{L}_{\text{recon}}
30:
                Update parameters by gradient descent on \mathcal{L}_{\mathrm{fine}}
31:
32: end for
33: 5. Inference
34: for all v_i \in \mathcal{V} do
                z_i \leftarrow g_{\gamma}(\hat{\mathbf{X}}, \hat{\mathbf{A}})[i,:]
s_i \leftarrow ||z_i||_2
35:
37: end for
38: Return \{s_i\} (ranked descending)
```

References

- Chaudhary, A.; Mittal, H.; and Arora, A. 2019. Anomaly detection using graph neural networks. In *Proceedings of the International Conference on Machine Learning, Big Data, Cloud and Parallel Computing*, 346–350.
- Chen, J.; Fu, S.; Ma, Z.; Feng, M.; Wirjanto, T. S.; and Peng, Q. 2025. Semi-supervised Anomaly Detection with Extremely Limited Labels in Dynamic Graphs. In *Proceedings of the International Conference on Database Systems for Advanced Applications*.
- Chen, J.; Fu, S.; Zhang, Z.; Ma, Z.; Feng, M.; Wirjanto, T. S.; and Peng, Q. 2024. Towards cross-domain few-shot graph anomaly detection. In *Proceedings of the IEEE International Conference on Data Mining*, 51–60. IEEE.
- Chen, X.; Chen, S.; Yao, J.; Zheng, H.; Zhang, Y.; and Tsang, I. W. 2020. Learning on attribute-missing graphs. *IEEE Transactions on Pattern Analysis and Machine Intelligence*, 44(2): 740–757.
- Ding, K.; Li, J.; Bhanushali, R.; and Liu, H. 2019a. Deep anomaly detection on attributed networks. In *Proceedings of the SIAM International Conference on Data Mining*, 594–602.
- Ding, K.; Li, J.; Bhanushali, R.; and Liu, H. 2019b. Deep Anomaly Detection on Attributed Networks. In *Proceedings of the SIAM International Conference on Data Mining*, 594–602.
- Duan, J.; Wang, S.; Zhang, P.; Zhu, E.; Hu, J.; Jin, H.; Liu, Y.; and Dong, Z. 2023. Graph anomaly detection via multiscale contrastive learning networks with augmented view. In *Proceedings of the AAAI Conference on Artificial Intelligence*, volume 37, 7459–7467.
- Fakhraei, S.; Foulds, J.; Shashanka, M.; and Getoor, L. 2015. Collective spammer detection in evolving multi-relational social networks. In *Proceedings of the ACM SIGKDD International Conference on Knowledge Discovery and Data Mining*, 1769–1778.
- Fu, S.; Peng, Q.; He, Y.; Du, B.; and You, X. 2023. Towards unsupervised graph completion learning on graphs with features and structure missing. In *Proceedings of the IEEE International Conference on Data Mining*, 1019–1024.
- He, J.; Xu, Q.; Jiang, Y.; Wang, Z.; and Huang, Q. 2024. Ada-gad: Anomaly-denoised autoencoders for graph anomaly detection. In *Proceedings of the AAAI Conference on Artificial Intelligence*, volume 38, 8481–8489.
- Huang, X.; Yang, Y.; Wang, Y.; Wang, C.; Zhang, Z.; Xu, J.; Chen, L.; and Vazirgiannis, M. 2022. Dgraph: A large-scale financial dataset for graph anomaly detection. In *Advances in Neural Information Processing Systems*, volume 35, 22765–22777.
- Huo, C.; Jin, D.; Li, Y.; He, D.; Yang, Y.-B.; and Wu, L. 2023. T2-gnn: Graph neural networks for graphs with incomplete features and structure via teacher-student distillation. In *Proceedings of the AAAI Conference on Artificial Intelligence*, volume 37, 4339–4346.
- Jiang, B.; and Zhang, Z. 2020. Incomplete graph representation and learning via partial graph neural networks. *arXiv* preprint arXiv:2003.10130.

- Jiang, X.; Qin, Z.; Xu, J.; and Ao, X. 2024. Incomplete graph learning via attribute-structure decoupled variational auto-encoder. In *Proceedings of the ACM International Conference on Web Search and Data Mining*, 304–312.
- Jin, M.; Liu, Y.; Zheng, Y.; Chi, L.; Li, Y.-F.; and Pan, S. 2021. Anemone: Graph anomaly detection with multi-scale contrastive learning. In *Proceedings of the ACM International Conference on Information and Knowledge Management*, 3122–3126.
- Kipf, T. N.; and Welling, M. 2016. Variational Graph Auto-Encoders. In *Advances in Neural Information Processing* Systems Workshop.
- Kumar, S.; Zhang, X.; and Leskovec, J. 2019. Predicting Dynamic Embedding Trajectory in Temporal Interaction Networks. In *Proceeding of the ACM SIGKDD International Conference on Knowledge Discovery and Data Mining*, 1269–1278.
- Li, J.; Gao, Y.; Lu, J.; Fang, J.; Wen, C.; Lin, H.; and Wang, X. 2025. DiffGAD: A Diffusion-based Unsupervised Graph Anomaly Detector. In *Proceedings of the International Conference on Learning Representations*.
- Liu, Y.; Li, Z.; Pan, S.; Gong, C.; Zhou, C.; and Karypis, G. 2022. Anomaly detection on attributed networks via contrastive self-supervised learning. *IEEE Transactions on Neural Networks and Learning Systems*, 33(6): 2378–2392.
- Luo, X.; Wu, J.; Beheshti, A.; Yang, J.; Zhang, X.; Wang, Y.; and Xue, S. 2022. Comga: Community-aware attributed graph anomaly detection. In *Proceedings of the ACM International Conference on Web Search and Data Mining*, 657–665
- Ma, X.; Wu, J.; Xue, S.; Yang, J.; Zhou, C.; Sheng, Q. Z.; Xiong, H.; and Akoglu, L. 2021. A comprehensive survey on graph anomaly detection with deep learning. *IEEE Transactions on Knowledge and Data Engineering*, 35(12): 12012–12038.
- Müller, E.; Sánchez, P. I.; Mülle, Y.; and Böhm, K. 2013. Ranking outlier nodes in subspaces of attributed graphs. In *Proceeding of the IEEE International Conference on Data Engineering Workshops*, 216–222.
- Pan, J.; Liu, Y.; Zheng, Y.; and Pan, S. 2023. PREM: A Simple Yet Effective Approach for Node-Level Graph Anomaly Detection. In *Proceedings of the IEEE International Conference on Data Mining*, 1253–1258.
- Park, S.; Lee, W.; Choe, B.; and Lee, S.-G. 2019. A survey on personalized PageRank computation algorithms. *IEEE Access*, 7: 163049–163062.
- Ruff, L.; Vandermeulen, R.; Goernitz, N.; Deecke, L.; Siddiqui, S. A.; Binder, A.; Müller, E.; and Kloft, M. 2018. Deep one-class classification. In *Proceedings of the International Conference on Machine Learning*, 4393–4402.
- Stekhoven, D. J.; and Bühlmann, P. 2011. MissForest—non-parametric missing value imputation for mixed-type data. *Bioinformatics*, 28(1): 112–118.
- Sánchez, P. I.; Müller, E.; Laforet, F.; Keller, F.; and Böhm, K. 2013. Statistical Selection of Congruent Subspaces for Mining Attributed Graphs. In *Proceeding of the IEEE International Conference on Data Mining*, 647–656.

- Tang, J.; Zhang, J.; Yao, L.; Li, J.; Zhang, L.; and Su, Z. 2008. ArnetMiner: extraction and mining of academic social networks. In *Proceeding of the ACM SIGKDD International Conference on Knowledge Discovery and Data Mining*, 990–998.
- Tu, W.; Zhou, S.; Liu, X.; Liu, Y.; Cai, Z.; Zhu, E.; Zhang, C.; and Cheng, J. 2022. Initializing Then Refining: A Simple Graph Attribute Imputation Network. In *Proceedings of the International Joint Conference on Artificial Intelligence*, 3494–3500.
- Xia, R.; Liu, H.; Li, A.; Liu, X.; Zhang, Y.; Zhang, C.; and Yang, B. 2025. Incomplete graph learning: A comprehensive survey. *Neural Networks*, 107682.
- Xiao, F.; and Fan, J. 2024. Unsupervised Anomaly Detection in The Presence of Missing Values. In *Proceedings of the Annual Conference on Neural Information Processing Systems*.
- Yang, Z.; Cohen, W.; and Salakhudinov, R. 2016. Revisiting semi-supervised learning with graph embeddings. In *Proceedings of the International Conference on Machine Learning*, 40–48.
- Yoon, J.; Jordon, J.; and van der Schaar, M. 2018. GAIN: Missing Data Imputation using Generative Adversarial Nets. In *Proceedings of the International Conference on Machine Learning*, volume 80, 5689–5698.
- Yu, S.; Dong, Z.; Wang, S.; Wan, X.; Liu, Y.; Liang, W.; Zhang, P.; Tu, W.; and Liu, X. 2024. Towards resource-friendly, extensible and stable incomplete multi-view clustering. In *Proceedings of the International Conference on Machine Learning*, 57415–57440.
- Yu, S.; Liu, S.; Wang, S.; Tang, C.; Luo, Z.; Liu, X.; and Zhu, E. 2025. Sparse low-rank multi-view subspace clustering with consensus anchors and unified bipartite graph. *IEEE Transactions on Neural Networks and Learning Systems*, 36(1): 1438–1452.
- Yuan, P.; and Tang, P. 2024. MDS-GNN: A Mutual Dual-Stream Graph Neural Network on Graphs with Incomplete Features and Structure. *arXiv* preprint arXiv:2408.04845.
- Zemicheal, T.; and Dietterich, T. G. 2019. Anomaly detection in the presence of missing values for weather data quality control. In *Proceedings of the ACM SIGCAS Conference on Computing and Sustainable Societies*, 65–73.
- Zeng, H.; Zhou, H.; Srivastava, A.; Kannan, R.; and Prasanna, V. 2020. Graphsaint: Graph sampling based inductive learning method. In *Proceeding of the International Conference on Learning Representations*.
- Zhang, G.; Li, Z.; Huang, J.; Wu, J.; Zhou, C.; Yang, J.; and Gao, J. 2022. efraudcom: An e-commerce fraud detection system via competitive graph neural networks. *ACM Transactions on Information Systems*, 40(3): 1–29.
- Zhang, S.; Yin, H.; Chen, T.; Hung, Q. V. N.; Huang, Z.; and Cui, L. 2020. Gcn-based user representation learning for unifying robust recommendation and fraudster detection. In *Proceedings of the International ACM SIGIR Conference on Research and Development in Information Retrieval*, 689–698.